A sustainable way of recycling polyamides: dissolution and ammonolysis of polyamides to diamines and diamides using ammonia and biosourced glycerol

Wouter Stuyck,[†] Kwinten Janssens,[†] Mats Denayer,[ꟼ] Free De Schouwer,[†] Robin Coeck,[†] Katrien V. Bernaerts,[‡] Jelle Vekeman,[§] Frank De Proft[ꟼ] & Dirk E. De Vos[†*]

[†]Centre for Membrane Separations, Adsorption, Catalysis and Spectroscopy for Sustainable Solutions (cMACS), KU Leuven, Celestijnenlaan 200F, post box 2454, 3001 Leuven, Belgium

[‡]Sustainable Polymer Synthesis Group, Aachen-Maastricht Institute for Biobased Materials (AMIBM), Faculty of Science and Engineering, Maastricht University, Brightlands Chemelot Campus, Urmonderbaan 22, 6167 RD Geleen, the Netherlands.

[ꟼ]Eenheid Algemene Chemie (ALGC), Department of Chemistry, Vrije Universiteit Brussel (VUB), Pleinlaan 2, 1050 Brussel, Belgium.

[§]Centre for Molecular Modeling (CMM), Ghent University, Technologiepark-Zwijnaarde 46, 9052 Zwijnaarde, Belgium.
E-mail: dirk.devos@kuleuven.be

Supplementary Information

1. Experimental details

1.1. Materials

Polyamide 66 (Sigma Aldrich, pellets), benzyl alcohol (Acros Organics, >99%), ethylene glycol (Acros Organics, 99.5%), glycerol (Acros Organics, >99%), diethylene glycol (Merck, 99%), 1,2-propanediol (Acros Organics, >99%), 1,3-propanediol (TCI, 98%), 2,3-butanediol (Fluka, 99%), 2,2,2-trifluoroethanol (Merck, 99%), tetrahydrofurfuryl alcohol (Merck, 98%), γ-butyrolactone (Acros, >99%), 4-methyl-1-cyclohexanol (Merck, 99%), 1-methyl-1-cyclohexanol (Merck, 96%), (R)-(+)-limonene (Merck, 97%), anisole (Merck, 99%), 1-heptanol (Merck, 98%), triethylene glycol (Fisher Scientific, 99%), tetraethylene glycol (J&K Scientific, 99.5%), toluene (Acros, >99.8%), formamide (Acros, 99.5%), 2-pyrrolidone (Fisher Scientific, 99%), phenol (Merck, >99%), m-cresol (VWR International, 99%), $NH_4H_2PO_4$ (Merck, >98%), CF_3SO_3H (TCI, 99%), $AlCl_3$ (Merck, 99%), $Al(OTf)_3$ (Sigma Aldrich, 99.9%), $Sn(OTf)_2$ (Acros, 98%), $FeCl_3$ (Merck, >99%), $Sc(OTf)_3$ (Sigma Aldrich, 99%), $Y(OTf)_3$ (Sigma Aldrich, 98%), $La(OTf)_3$ (Sigma Aldrich, 99.999%), $LaCl_3$

(Thermo Fisher, 99.9%), Yb(OTf)$_3$ (Sigma Aldrich, 99.9%), (NH$_4$)$_2$Ce(IV)(NO$_3$)$_6$ (Sigma Aldrich, 99.99%), Zr(acac)$_4$ (Merck, 98%), TiCl$_4$ (Acros Organics, 99.9%), TiO$_2$ (Merck, nanopowder <100 nm particle size, 99%), CeO$_2$ (Alfa Aesar, 99.5%), CD$_3$OD (Merck, 99.8%), NH$_3$ (Air Liquide, N38), N$_2$ (Air Liquide, α1), hexamethylene diamine (Fisher Scientific, >99.5%), adipamide (TCI, >98.0%), acetamide (Acros Organics, 99%), 2-methylimidazole (Merck, 99%), *N,O*-Bis(trimethylsilyl)trifluoroacetamide (BSTFA) (TCI, >95.0%) and crude glycerol (Oleon NV, ex-biodiesel production).

1.2. Dissolution of polyamide 66

To investigate the dissolution of polyamide 66, 0.5 mmol of polyamide 66 was added to a glass vial (1.8 mL) together with 1 mL of a solvent. Subsequently, the vial was placed in a heating block at 180 °C under continuous stirring for 20 hours. For some solvents, the temperature had to be kept lower due to a low boiling point of the solvent. The dissolution of polyamide 66 was achieved when no polymer flakes were visible after the experiment.

1.3. Ammonolysis of polyamide 66

All ammonolysis reactions were performed in a 20 mL pressure Parr batch reactor. In a typical ammonolysis experiment, 1 mmol of polyamide 66 (0.1 M, 0.2624 g) was added to the reactor together with 10 mL glycol solvent (ethylene glycol or glycerol) and 5 mol% lanthanum(III) triflate (La(OTf)$_3$). In addition, 0.1 M of benzyl alcohol (104 μL) was added as an internal standard for quantification of the number of broken polyamide bonds *via* ^{1}H-NMR and the number of hexamethylenediamine monomers via gas chromatography. Subsequently, the reactor was sealed, purged with N$_2$, pressurized with 1 bar NH$_3$, and heated to 200 °C for a reaction time of 20 hours under continuous stirring. For the reverse reaction, 1 mmol of hexamethylenediamine (0.1 M, 0.1159 g) and 1 mmol of adipamide (0.1 M, 0.1442 g) were applied in ethylene glycol under the same conditions.

1.4. Estimation of the NH_3 concentration in ethylene glycol and glycerol

To determine the concentration of NH_3 in the applied solvent for a certain pressure, the Parr batch reactor was weighed prior and after loading it with NH_3. The difference in mass will be denoted as $m(NH_3)$:

$$m(NH_3) = m(Reactor_{Prior}) - m(Reactor_{After}) \quad (1)$$

The mass of NH_3 that is present in the reactor is related to the amount of NH_3 that is dissolved in the solvent ($n(NH_{3,sol})$) via following formula:

$$n(NH_{3,gas}) + n(NH_{3,sol}) = \frac{m(NH_3)}{M(NH_3)} \quad (2)$$

Where $M(NH_3)$ denotes the molar mass of NH_3. Dividing this by the volume of the solvent and rearranging the formula then gives an estimation of the concentration of NH_3 in the solution ($c(NH_{3,sol})$).

$$c(NH_{3,sol}) = \frac{m(NH_3)}{M(NH_3) * V(solvent)} - \frac{n(NH_{3,gas})}{V(solvent)} \quad (3)$$

To estimate the amount of NH_3 that is present in the gas phase ($n(NH_{3,gas})$), the ideal gas law can be applied. The total volume of the reactor is approximately 31.25 mL and since 10 mL is already occupied by solvent, 21.25 mL remains as the volume where NH_3 can be present as a gas (V(gas)).

$$p * V(gas) = n(NH_{3,gas}) * R * T \quad (4)$$

Where p is the operational pressure during the ammonolysis process. For a typical reaction in ethylene glycol where an initial pressure of 1 bar NH_3 was applied at room temperature, the operational pressure amounted 18 bar at 473.15 K (200 °C). By rearranging and filling in the correct values for this example in formula (4), $n(NH_{3,gas})$ can be calculated.

$$n(NH_{3,gas}) = \frac{18 * 10^5 Pa * 21.25 * 10^{-6} m^3}{8.314 \, J \, mol \, K^{-1} * 473.15 \, K} = 9.7 * 10^{-3} \, mol \quad (5)$$

Now, the concentration of NH_3 ($c(NH_{3,sol})$) can be calculated by filling in $n(NH_{3,gas})$ and $M(NH_3)$ in formula (3). The mass of NH_3 in this particular example was 3.2 gram.

$$c(NH_3) = \frac{3.2\ g}{17.031\ g\ mol^{-1} * 0.01\ L} - \frac{9.7 * 10^{-3} mol}{0.01\ L} = 18\ M \qquad (6)$$

1.5. Product analysis by ^{1}H-NMR

To grade the performance of the ammonolysis reactions, the number of broken polyamide bonds was selected as the criterion, which was estimated by liquid ^{1}H-NMR. After centrifugation, 200 µL of the crude reaction mixture was mixed with 300 µL CD$_3$OD and transferred to an NMR tube. ^{1}H-NMR spectra were recorded on a Bruker Avance 400 MHz spectrometer equipped with a sample case and a 5 mm PABBO BB/19F-1H/D probe with z-gradients and ATM accessory for Automatic Tuning and Matching. The large signal of the applied solvent was suppressed by an adjusted zgpr pulse program: p1 = 8 µs; plw1 = -1 db; plw9 = 50 db; ds = 2; ns = 32; d1 = 5 s; aq = 1.98 s; sw = 20 ppm; o1P on the resonance signal of the applied solvent (Table S1). When glycerol is applied as the solvent in the ammonolysis experiment, the repetition time (d1) was increased to 20 s for quantitative analysis. In addition, ^{1}H,^{1}H-COSY, ^{1}H,^{13}C-HSQC and ^{1}H,^{13}C-HMBC 2D Liquid NMR spectra were recorded on the same equipment for product identification.

Table S1. Chemical shift of the suppressed solvent signal in the zgpr pulse program

| Solvent	Chemical shift of signal to be suppressed [ppm]
Ethylene glycol	3.62
Diethylene glycol	3.58
1,3-propanediol	3.67
1,2-propanediol	3.55
Glycerol	3.63
Water	3.63
2,2,2-trifluoroethanol	3.87
Tetrahydrofurfuryl alcohol	3.53
Dioxane	3.67

A typical ^{1}H-NMR spectrum of a crude reaction mixture is shown in Figure S1 together with the assignment of the peaks to the corresponding protons of the polyamide. Complete identification of all the peaks is provided in the section product identification. The percentage of broken polyamide bonds was calculated from the distinct triplet signal of the generated primary amine after the secondary amide bond was broken by NH_3 (Figure S1, pink, A'(Primary amines)). Benzyl alcohol served as an internal standard for this by using the signal of its aromatic protons (δ = 7.20 ppm – 7.40 ppm, m, 5H, A'(Benzyl alcohol), not shown). First, the concentration of primary amines was calculated by following formula:

$$c(Primary\ amines) = \frac{5}{2} * \frac{A'(Primary\ amines)}{A'(Benzyl\ alcohol)} * c(Benzyl\ alcohol)$$

Next the percentage of broken polyamide bonds was derived from the concentration of the primary amines and the initial concentration of secondary amide bonds (c(secondary amides)$_0$) by following formula:

$$Percentage\ of\ broken\ polyamide\ bonds\ (\%) = \frac{c(Primary\ amines)}{c(secondary\ amides)_0} * 100$$

The concentration of primary amide bonds after the ammonolysis experiment could not be determined quantitatively since the solvent peak coincided with the signal of the secondary amide bonds (-CONH-C$\underline{H}_2$-) (Figure S1, grey).
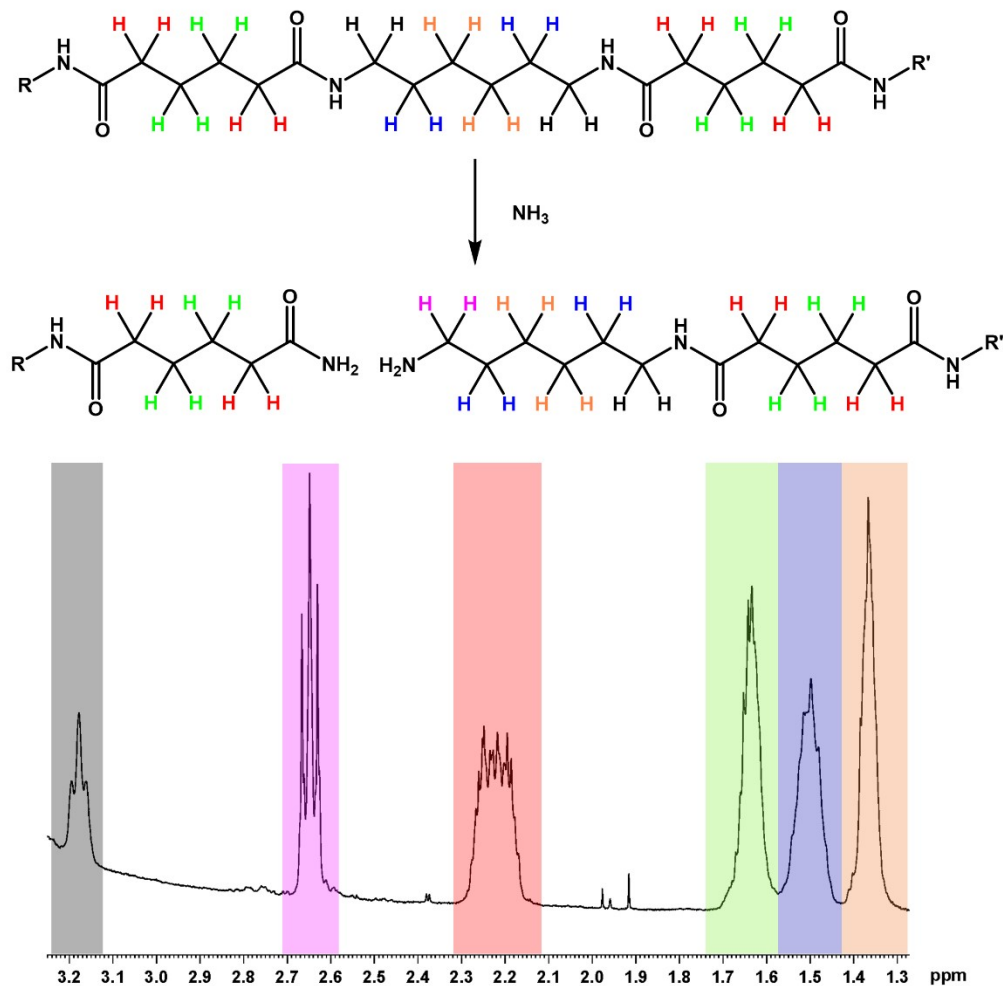
Figure S1. Typical ^{1}H-NMR spectrum of a crude reaction mixture (bottom) together with the assignment of the peaks to the corresponding protons of the polyamide (top).

1.6. Product analysis by gas chromatography (GC) coupled with mass spectrometry (GC-MS)

After centrifugation, the crude reaction mixture was analyzed on a Shimadzu GC-2010 instrument equipped with a CP-SIL 5 CB column and FID detector to determine the amount of free hexamethylenediamine and potentially other small side products. All unknown products were identified with GC-MS performed on an Agilent 6890N GC instrument, equipped with a HP-5 MS column, coupled to a 5973N mass spectrometer. In an attempt to also characterize heavier and more polar compounds a liquid aliquot (50 μL) was derivatized using 450 μL *N,O*-Bis(trimethylsilyl)trifluoroacetamide (BSTFA). Full derivatisation was obtained after stirring the reaction mixture for 1h at 70°C. All identified side products

are reported in section 1.7. and were below 1% in product yield. In the case of pure glycerol reactions the samples proved to be too viscous. This was easily circumvented by diluting the reaction sample in ethanol (1:1 ratio). Monomer yields were readily obtained using Benzyl alcohol as the internal standard (already present as the standard for the NMR analysis). Quantitative product analysis was performed using the effective carbon number (ECN).

1.7. Product identification by NMR and GC MS of reactions in ethylene glycol or glycerol

Ammonolysis polyamide 66 to primary amide and primary amine
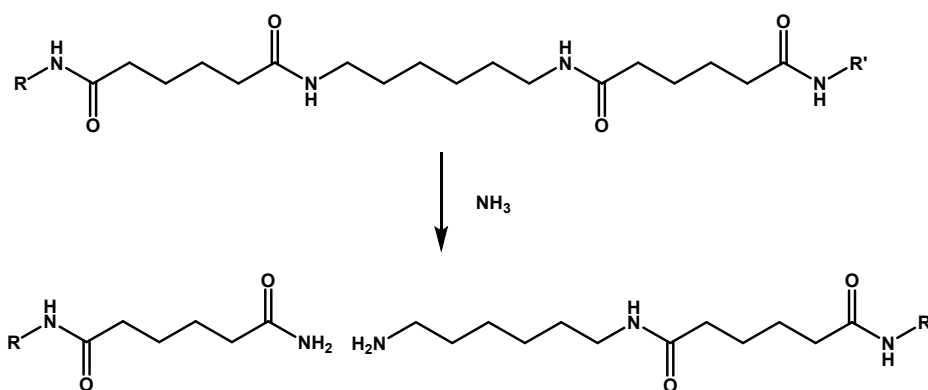
^{1}H-NMR (400 MHz, CD$_3$OD): δ (ppm) = 3.18 (t, ^3J = 6.77 Hz, 4H; -CONH-C$\underline{H}_2$-), 2.64 (t, ^3J = 6.77 Hz, 2H; -C$\underline{H}_2$-NH$_2$), 2.34 (m, 4H; -C$\underline{H}_2$-CONH-, 2H; -C$\underline{H}_2$-CONH$_2$), 1.64 (m, 4H; -C$\underline{H}_2$-CH$_2$-CONH-, 2H; -C$\underline{H}_2$-CH$_2$-CONH$_2$), 1.50 (m, 4H; -C$\underline{H}_2$-CH$_2$-NHCO-, 2H; -C$\underline{H}_2$-CH$_2$-NH$_2$), 1.36 (m, 4H; -C$\underline{H}_2$-CH$_2$-CH$_2$-NHCO-, 2H; -C$\underline{H}_2$-CH$_2$-CH$_2$-NH$_2$)

Nitrile function
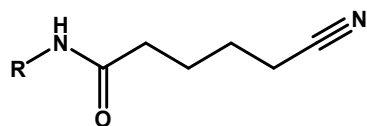
^{1}H-NMR (400 MHz, CD$_3$OD): δ (ppm) = 2.51 (t, ^3J = 7.12 Hz, 2H; -CH$_2$-C$\underline{H}_2$ -CN), 2.34 (m, 2H; -C$\underline{H}_2$-CONH-), 1.67 (m, 2H; -C$\underline{H}_2$-CH$_2$-CN), 1.64 (m, 2H; -C$\underline{H}_2$-CH$_2$-CONH-).

^{13}C{^{1}H}-NMR (400 MHz, CD$_3$OD): δ (ppm) = 177.7 (1C, -$\underline{C}$ONH-), 120.1 (1C, -$\underline{C}$N), 34.8 (1C, $\underline{C}$H$_2$-CONH-), 25.1 (1C, $\underline{C}$H$_2$-CH$_2$-CONH-), 24.8 (1C, NC-CH$_2$-$\underline{C}$H$_2$-), 15.8 (1C, NC-$\underline{C}$H$_2$-).

Imidazole function
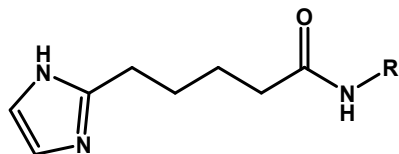
^{1}H-NMR (400 MHz, CD$_3$OD): δ (ppm) = 6.93 (s, 2H; -NH-C**H**=C**H**-N=), 2.74 (t, 2H; C-C**H**$_2$-CH$_2$-CH$_2$-CONH-), 2.34 (m, 2H; -C**H**$_2$-CONH-), 1.73 (m, 2H, -C**H**$_2$-CH$_2$-CH$_2$-CONH-), 1.64 (m, 2H, -C**H**$_2$-CH$_2$-CONH-)

^{13}C{^{1}H}-NMR (400 MHz, CD$_3$OD): δ (ppm) = 177.7 (1C, -**C**ONH-), 148.2 (1C, (NH)(N)**C**-CH$_2$-), 122.3 (2C, -NH-**C**H=**C**H-N=), 34.8 (1C, -**C**H$_2$-CONH-), 27.2 (1C, (NH)(N)C-**C**H$_2$-CH$_2$), 25.1 (1C, -CH$_2$-**C**H$_2$-CONH-), 24.5 (1C, -**C**H$_2$-CH$_2$-CH$_2$-CONH-).

Ethylene glycol (MW = 62 g/mol)
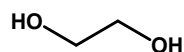
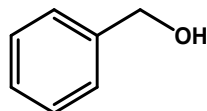^{1}H-NMR (400 MHz, CD$_3$OD): δ (ppm) = 3.62 (s, 4H; C**H**$_2$-OH)

GC/MS (EI, 70 eV): m/z (rel. int., %): 62 (9), 44 (6), 43 (26), 42 (14), 33 (28), 32 (8), 31 (100), 30(11), 29 (56).

Glycerol (MW = 92 g/mol)
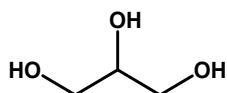
^{1}H-NMR (400 MHz, CD$_3$OD): δ (ppm) = 3.69 (m, 1 H; >C**H**-OH), 3.62 (m, 2 H; C**H**$_2$-OH), 3.54 (m, 2 H; C**H**$_2$-OH)

Benzyl alcohol (MW = 108 g/mol)

^{1}H-NMR (400 MHz, CD$_3$OD): δ (ppm) = 7.45 - 7.23 (m, 5H, C$_6$**H**$_5$-CH$_2$OH), 4.63 (s, 2H; -C**H**$_2$OH)

GC/MS (EI, 70 eV): m/z (rel. int., %): 109 (7), 108 (82), 107 (60), 105 (5), 91 (16), 90 (7), 89 (9), 80(11), 79 (100, 78 (16), 77 (62), 74 (7), 65 (7), 63 (9), 62 (5), 52 (5), 51 (21), 50 (14), 39 (7).

Hexamethylenediamine (MW = 116 g/mol)
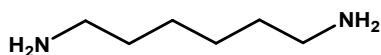
GC/MS (EI, 70 eV): m/z (rel. int., %): 100 (13), 99 (10), 98 (5), 87 (29), 86 (17), 72 (7), 70 (17), 69 (9), 59 (7), 57 (6) 56 (42), 55 (8), 45 (9), 44 (11), 43 (11), 42 (15), 41 (13), 39 (8), 31 (6), 30 (100).
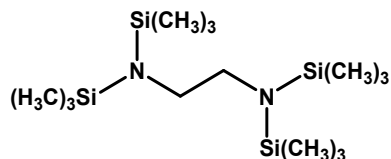
2,2,10,10-tetramethyl-3,6,9-trioxa-2,10-disilaundecane (MW = 250 g/mol)
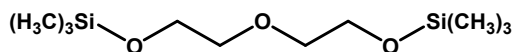
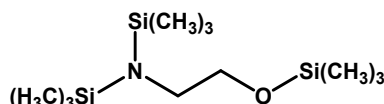GC/MS (EI, 70 eV): m/z (rel. int., %): 191 (5), 189 (15), 148 (10), 147 (44), 145 (6), 133 (11), 118 (7), 117

(84), 116 (34), 103 (21), 101 (9), 75 (18), 73 (100), 59 (9), 45 (12).

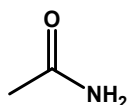**N^1,N^1,N^2,N^2-tetrakis(trimethylsilyl)ethane-1,2-diamine (MW = 348 g/mol)**

GC/MS (EI, 70 eV): m/z (rel. int., %): 176 (9), 175 (20), 174 (100), 148 (18), 133 (11), 100 (12), 73 (35).

1,1,1-trimethyl-*N*-(trimethylsilyl)-*N*-(2-((trimethylsilyl)oxy)ethyl)silaneamine (MW = 277 g/mol)
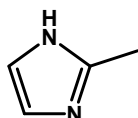

GC/MS (EI, 70 eV): m/z (rel. int., %): 176 (8), 175 (18), 174 (100), 147 (15), 133 (10), 100 (10), 86 (7), 73 (28).

Acetamide (MW = 59 g/mol)

^{1}H-NMR (400 MHz, CD$_3$OD): δ (ppm) = 1.97 (s, 3H; C$\underline{H}_3$-CONH$_2$),

2-Methylimidazole (MW = 82 g/mol)

^{1}H-NMR (400 MHz, CD$_3$OD): δ (ppm) = 6.91 (s, 2H; -NH-C$\underline{H}$=C$\underline{H}$-N=), 2.37 (s, 3H; -C-C$\underline{H}_3$)

GC/MS (EI, 70 eV): m/z (rel. int., %): 83 (5), 82 (100), 81 (5), 55 (9), 54 (35), 52 (7), 42 (13), 41 (13), 40 (9).

1.8. Crude Glycerol analysis

Ex-biodiesel crude glycerol was kindly provided by OleonNV (±80 wt% glycerol).[1] Additional experiments were performed to analyze the composition of the industrial glycerol. The industrial sample was simply filtered over a 0.45 µm filter (Merck, Millipore Millex HP) to remove solid particles, obtaining a homogeneous, amber colored liquid. The viscosity was determined with the help of Luca Passaro using a double wall Couette geometry installed on an ARES-G2. A flow sweep test was performed at 20°C following a logarithmic growth of shear rate applied from 1-100 s^{-1}, resulting in a viscosity of 56±1 mPa*s.

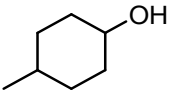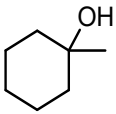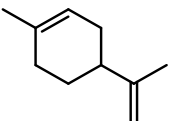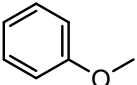Karl Fisher titration was performed (870 KF Titrino plus, Metrohm) indicating 20±1 wt% water. Chloride content was determined via Volhard titration indicating a total chloride content of 2 wt%.

2. Dissolution of PA66

Dissolution of the rigid semi-crystalline PA66 polymer matrix can be achieved at room temperature in hydroxy-aromatics,[2-5] strong acids,[2,4-6] halogenated alcohols[8,9] or inorganic salts in methanol.[2,8,9] Each of these solvents can interact with the strong hydrogen bonds that link the individual polymer chains of the PA66 plastic together, and thereby dissolving PA66 at room temperature. In the case of hydroxy-aromatics, strong acids and the halogenated alcohols, a strongly acidic proton can interact with the proton accepting carbonyl oxygen atoms of the secondary amide bonds *via* acid-base interactions or hydrogen bond formation. For the inorganic salts dissolved in methanol, the Lewis acid cation can coordinate with carbonyl oxygen atom of the secondary amide bond and thereby weaken the hydrogen bonds between the different PA66 chains. However, each of these systems poses major drawbacks such as incompatibility with ammonia or very corrosive or toxic mixtures. Therefore, this work envisages the use of a green alternative to abovementi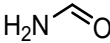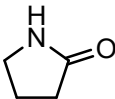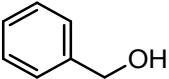oned solvent systems to dissolve the PA66 plastic at a relatively mild temperature of 180 °C, unless a lower temperature had to be applied as a result of the low boiling point of the applied solvent. In this study, biobased derivatives from hydroxy-aromatics and other proton donating solvents like alcohols, diols, triols and amides were included (Table S2).

Table S2. Investigation of the dissolution of PA66 in different solvents
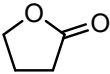
Solvent	Structure	Temperature (°C)	PA66 Dissolution
γ-Butyrolactone		180	✗
Tetrahydrofurfuryl alcohol		180	✗
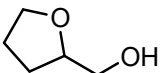
Solvent	Structure	Temperature (°C)	PA66 Dissolution
4-Methylcyclohexanol		180	✗
1-Methylcyclohexanol		180	✗
Limonene		180	✗
Anisole		180	✗
1-Heptanol		180	✗
Triethylene glycol		180	✗
Tetraethylene glycol		180	✗
Tetrahydrofuran		60	✗
Cyclopentyl methyl ether		140	✗
Toluene		140	✗
Formamide		180	✓
2-Pyrrolidone		180	✓
Benzyl alcohol		180	✓
Ethylene glycol		180	✓
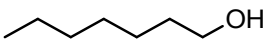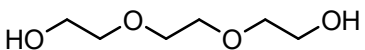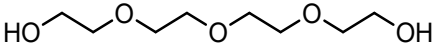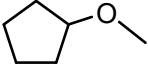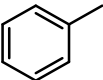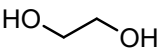
Solvent	Structure	Temperature (°C)	PA66 Dissolution
1,2-Propanediol		180	
1,3-Propanediol		180	
Glycerol		180	
2,3-Butanediol		180	
Diethylene glycol		180	
Phenol		70	
		140	
m-Cresol		70	
		140	
30/70 phenol/anisole		140	
30/70 phenol/toluene		70	
		140	
50/50 toluene/ 4-methyl-cyclohexanol		140	✗

Conditions: 0.05 M PA66 is added to a glass vial with 1 mL of solvent for 20 h at indicated temperatures.

Non-toxic and biobased derivatives of phenol, like 4-methylcyclohexanol and 1-methylcyclohexanol, are unable to dissolve PA66 at 180 °C, which suggests that the aromatic structure is essential to dissolve PA66. On the other hand, aromatics like toluene and anisole are likewise unable to dissolve PA66, while phenol and m-cresol dissolve PA66 even at 70 °C, which indicates that the proton donating effect of hydroxy

aromatics is also an important factor for the dissolution ability of the solvent. A 50/50 toluene/4-methylcyclohexanol mixture doesn't dissolve PA66, while a 30/70 phenol/anisole mixture does, which demonstrates that especially the proton donating character of the solvent is important. This hypothesis is confirmed by the successful dissolution of PA66 in other proton donating solvents like small diols (ethylene glycol, 1,2-propanediol, 1,3-propanediol, 2,3-butanediol and diethylene glycol), glycerol and amides (formamide and 2-pyrrolidone) at 180 °C, while ethereal solvents (cyclopentyl methyl ether and tetrahydrofuran) are unable to dissolve PA66. When the length of the diol increases (like for triethylene glycol and tetraethylene glycol), the protic character of the solvent decreases, which leads to the inability of these solvents to dissolve PA66. Although formamide and 2-pyrrolidone successfully dissolve PA66, they are unsuitable in this work since they would interfere with the secondary amide bonds of PA66 during the ammonolysis process. From the results of this study, ethylene glycol was selected as a suitable and green solvent to perform the ammonolysis of PA66 at 200 °C.

3. Influence of NH_3 pressure on the ammonolysis of PA66

Table S3. Influence of NH_3 pressure on the ammonolysis of PA66

NH_3 pressure [bar]	Concentration NH_3 [M]	Broken PA66 bonds [%]
0.5	13	44
1.0	18	53
2.0	26	51
4.0	39	57

Conditions: 0.1 M PA66 and 0.1 M benzyl alcohol (internal standard) in ethylene glycol (10 mL), 200 °C, 5 mol% La(OTf)$_3$, 20 h.

4. Influence of the reaction temperature on the ammonolysis of PA66

Increasing the reaction temperature to 220 °C led to an increase of the amount of broken polyamide bonds (Table S4). However, this increase also led to a more significant fraction of side products, which could be identified by performing a reaction with adipamide as the substrate, as nitrile and imidazole

functions by 2D liquid ^{1}H-^{1}H NMR and ^{1}H-^{13}C NMR analyses (Figure S3 – Figure S5 & section 1.5). Whereas the nitrile functions can be generated *via* dehydration of the primary amides present in the reaction mixture,[10] the presence of the imidazole function is far less evident. We postulate that this imidazole function is generated from a nitrile group (for instance from 5-cyanovaleramide) which will react with ethylene diamine (**A**) to an amidine function (**B**) (Figure S6). Ethylene diamine itself originates from the exchanges of NH_3 with the hydroxyl groups of ethylene glycol and was detected in the reaction mixtures by gas chromatography coupled mass spectroscopy analysis after derivatization with *N,O*-Bis(trimethylsilyl)trifluoroacetamide (BSTFA) (section 1.7). A second nucleophilic attack of the remaining primary amine leads to cyclization (**C**), after which elimination of NH_3 will lead to the generation of an imidazoline (**D**).[11,12] In a last step, the aromatic ring will be restored and an imidazole structure will be generated (**E**). To confirm this hypothesis, acetamide was applied as a substrate under normal ammonolysis conditions, which lead to the clear production of 2-methyl imidazole (Figure S7).

Table S4. Influence of temperature on product distribution of the ammonolysis of PA66 in ethylene glycol

T [°C]	Broken PA66 bonds [%]	Nitrile functions [%]	Imidazole functions [%]
200	53	3	9
220	62	2	19

Conditions: 0.1 M PA66 in and 0.1 M benzyl alcohol (internal standard) ethylene glycol (10 mL), 5 mol% La(OTf)$_3$, 1 bar NH_3, 20 h.
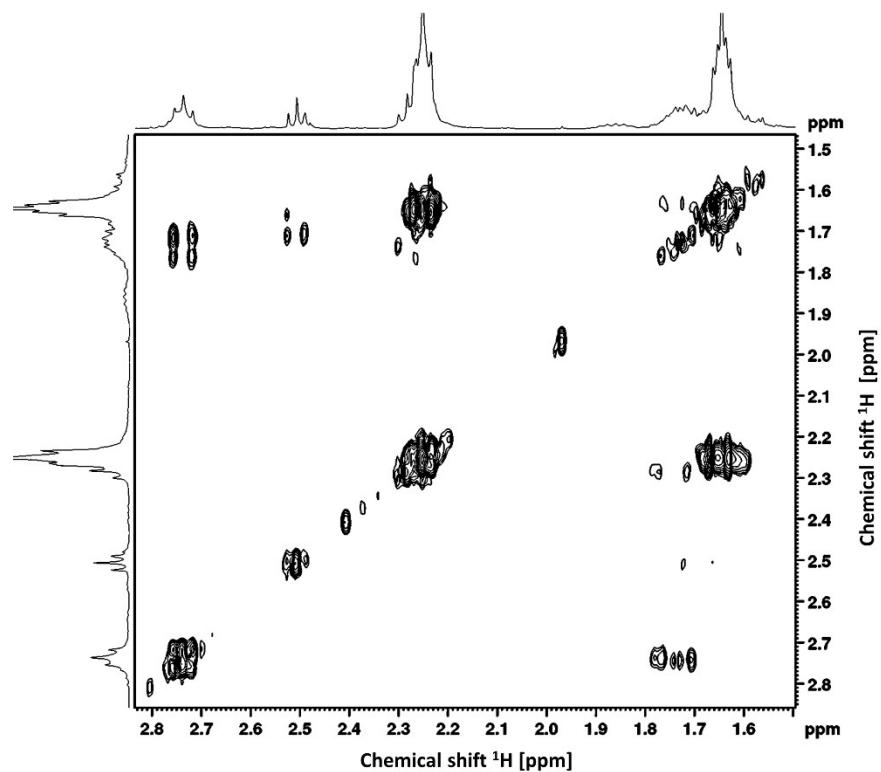
Figure S2. ^{1}H-^{1}H COSY spectrum of the crude reaction mixture when 0.1 M adipamide is applied in ethylene glycol under standard ammonolysis conditions.
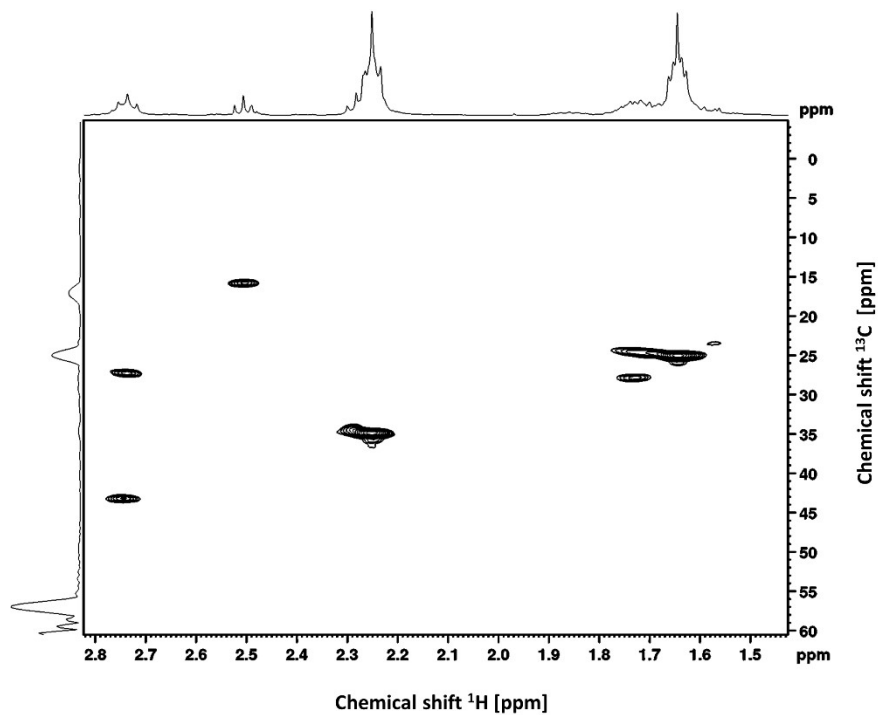
Figure S3. ^{1}H-^{13}C HSQC spectrum of the crude reaction mixture when 0.1 M adipamide is applied in ethylene glycol under standard ammonolysis conditions.
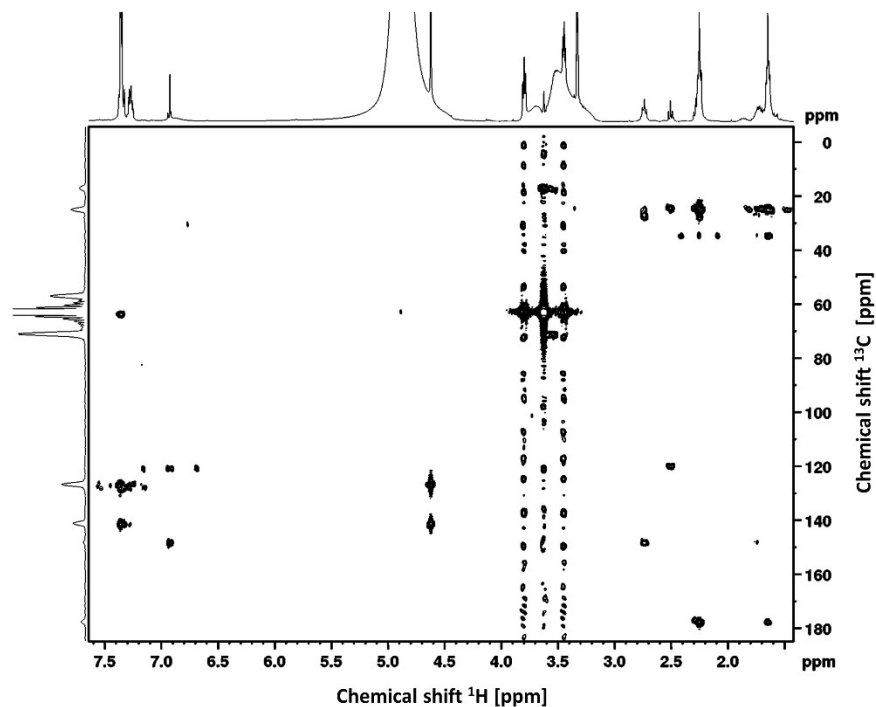
Figure S4. ^{1}H-^{13}C HMBC spectrum of the crude reaction mixture when 0.1 M adipamide is applied in ethylene glycol under standard ammonolysis conditions.

1. Generation ethylene diamine
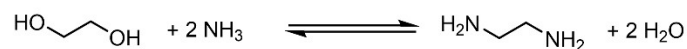
2. Dehydration adipamide to 5-cyanovaleramide
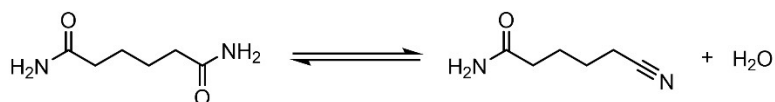
3. Generation imidazole function

Figure S5. Reaction equations and possible mechanisms for the observed nitrile and imidazole functions in the crude mixtures of the ammonolysis of 0.1 M PA66 in ethylene glycol (10 mL) at 220 °C and with 1 bar NH_3.

Figure S6. Liquid ^{1}H-NMR spectrum of the crude reaction mixture with acetamide as the substrate, with assignment of the acetamide and 2-methylimidazole peaks. The two large peaks at 4.75 ppm and 3.52 ppm originate from ethylene glycol and the peaks at 7.45 ppm – 7.23 ppm originate fr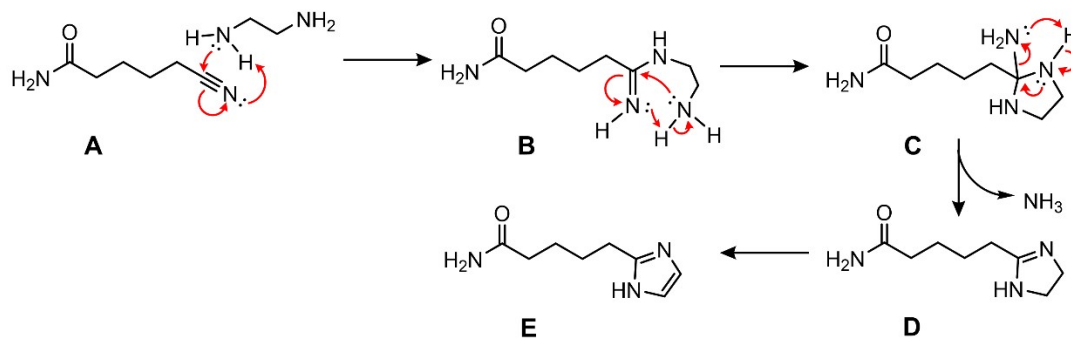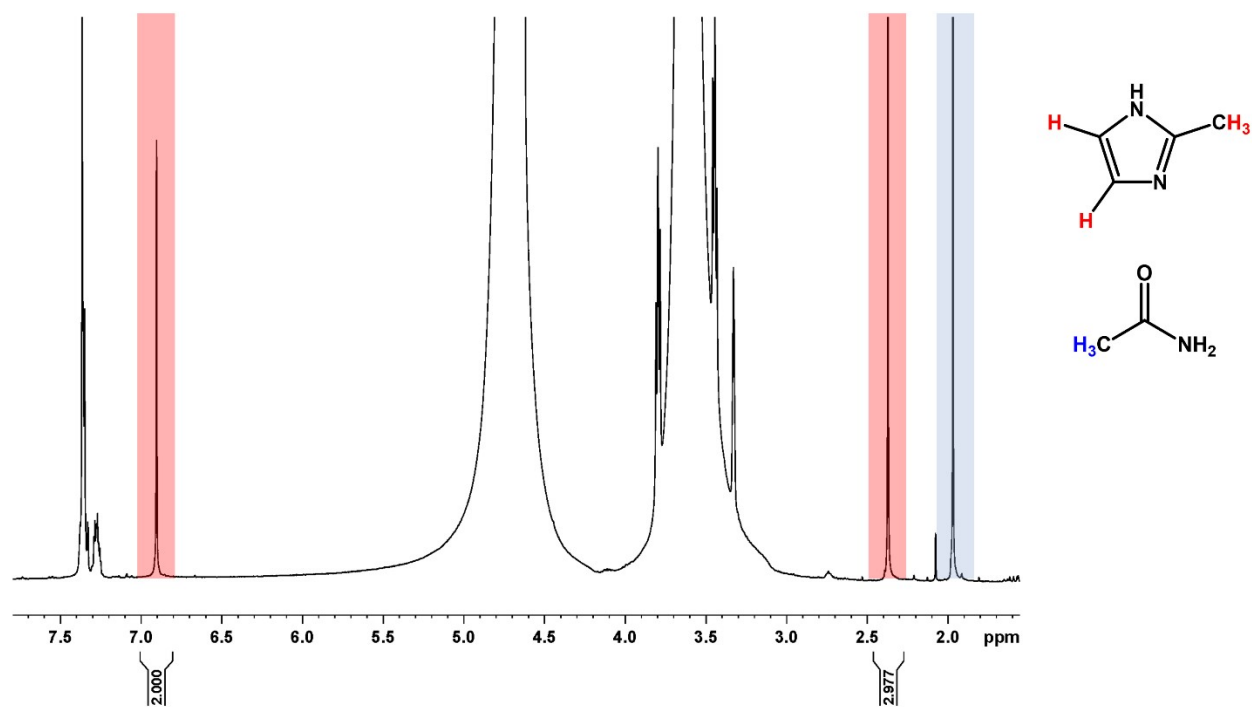om the internal standard benzyl alcohol. Reaction conditions: 0.1 M acetamide in ethylene glycol (10 mL), 5 mol% La(OTf)$_3$, 200 °C, 1 bar NH$_3$, 20 h.

5. Gel permeation chromatography

The molar mass and the polymer dispersity were determined with size exclusion chromatography (SEC).

To this end, in 1.5 ml 1,1,1,3,3,3-hexafluoro isopropanol containing 0.019 % sodium trifluoroacetate, 5 mg

of the reaction mixture was dissolved and filtered over a 0.2 μm Teflon syringe filter. For the calibration

curve, poly(methyl methacrylate) standards with a molar mass ranging from 831 to 1 890 000 g/mol were

used. First, a precolumn PFG combination medium with 7 μm particle size (4.6 x 30 mm) was used and

thereafter two PFG combination medium microcolumns with 7 μm particle size (4.6 x 25 mm, separation

range 100 – 1 000 000 g/mol), in combination with a refractive index detector. The spectra were analyzed

with the PSS WinGPC UniChrom software.
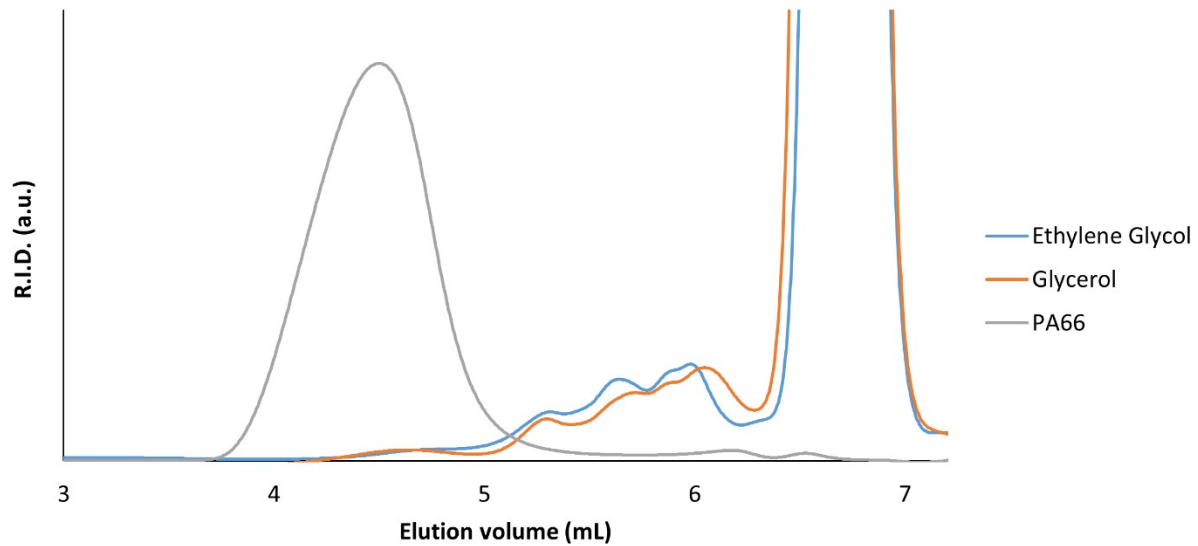
Figure S7. GPC elution chromatogram (elution rate 0.330 mL/min) of the unreacted PA66 substrate (grey) and the ammonolysis reaction mixtures with ethylene glycol (blue) and glycerol (orange) as the applied solvent.

Code	M_n (g/mol)	Đ
PA66	25200	2.30
Ethylene glycol	1070	2.62
Glycerol	900	5.29
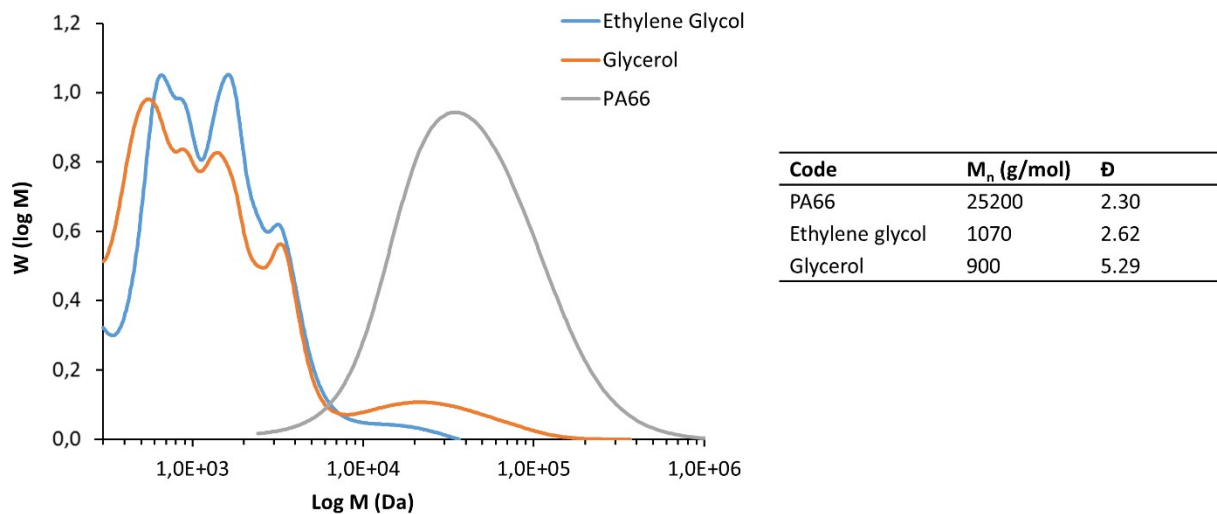
Figure S8. GPC molar mass distributions (left) and calculated number average molar mass and dispersity (right) of the unreacted PA66 substrate (grey) and the ammonolysis reaction mixtures with ethylene glycol (blue) and glycerol (orange) as the applied solvent.

6. Ammonolysis equilibrium

Table S5. Forward and reverse ammonolysis reaction in ethylene glycol and glycerol.
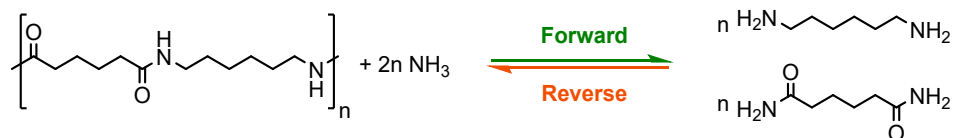
Type	T [°C]	Solvent	Catalyst	Primary amines [%][a]	Secondary amides [%][b]
Forward	200	Ethylene glycol	5 mol% La(OTf)$_3$	53	47
Forward	200	Ethylene glycol	50 mol% La(OTf)$_3$	66	34
Forward	200	Glycerol	5 mol% La(OTf)$_3$	69	31
Forward	200	Glycerol	/	66	34
Reverse	200	Ethylene glycol	5 mol% La(OTf)$_3$	68	32
Reverse	200	Glycerol	5 mol% La(OTf)$_3$	67	33

Conditions forward reaction: 0.1 M PA66 and 0.1 M benzyl alcohol (internal standard) in solvent (10 mL), 1 bar NH$_3$, 20 h. Conditions reverse reaction: 0.1 M hexamethylenediamine and 0.1 M adipamide and 0.1 M benzyl alcohol (internal standard) in solvent (10 mL), 1 bar NH$_3$, 20 h. [a] The amount of primary amines equals the number of broken bonds for the forward reactions. . [b] The amount of secondary amides equals the number of bonds that are left intact for the forward reactions, or the amount of generated secondary amide bonds during the reverse reactions, and are calculated by subtracting the percentage of primary amines from 100%.

7. Hexamethylene diamine yield

Table S6. Amount of broken PA66 bonds compared to the monomer yield for a various set of ammonolysis reactions.[a]

Catalyst	Time	NH$_3$ [bar]	Solvent	T [°C]	Broken PA66 bonds/ Monomer yield [%]	Ref. [b]
LaCl$_3$	20 h	1	Ethylene glycol	200	53	-
La(OTf)$_3$	20 h	1	Ethylene	200	53	-

			glycol			
La(OTf)$_3$	20 h	4	Ethylene glycol	200	57	-
La(OTf)$_3$	20 h	1	Ethylene glycol	220	62	-
-	20 h	1	Glycerol	200	69	-
-	20 h	1	Crude Glycerol [c]	200	68	-
(NH$_4$)$_2$HPO$_4$ [d]	90 min	Liquid [e]	-	320	18 [f]	13
TiI$_4$ [g]	30 min	Liquid [e]	-	300	44 [f]	14
ScCl$_3$ [g]	30 min	Liquid [e]	-	300	44 [f]	14
Nb$_2$O$_5$ (HT Parr) & RuWO$_x$/MgAl$_2$O$_4$ [h]	16 h	6	CPME	200	36 [i]	15

[a] Conditions for reactions performed in this work: 0.1 M PA66 and 0.1 M benzyl alcohol (internal standard) in solvent (10 mL), 5 mol% catalyst. [b] References. [c] Filtered crude glycerol. [d] 2 wt% (NH$_4$)$_2$HPO$_4$. [e] Ammonia is applied as a liquid. [f] Hexamethylene diamine. [g] 1 wt% TiI$_4$ and 1 wt% ScCl$_3$. [h] 228 wt% Nb$_2$O$_5$ (HT Parr) & 38 wt% RuWO$_x$/MgAl$_2$O$_4$ (4 wt% Ru, molar ratio Ru-W of 8-1). [i] Azepane.

8. Computational approach

The optimal static configuration of the amide-ammonia-glycerol/1,3-propanediol complex was found by calculating the radial distribution functions (RDFs) derived from classical molecular dynamics (MD) simulations using the GROMACS package and the OPLS-AA force-field. The radial distribution function between A (reference) and B is defined as

$$g(r) = \frac{\rho(r)}{\rho_0}$$

where $\rho(r)$ is the number density of B at distance r from A, and ρ_0 is the bulk density of B.

Two MD simulations were carried out. In one simulation, an in vacuum geometry optimized amide-ammonia dimer (Figure S9) was solvated in glycerol, while keeping the reac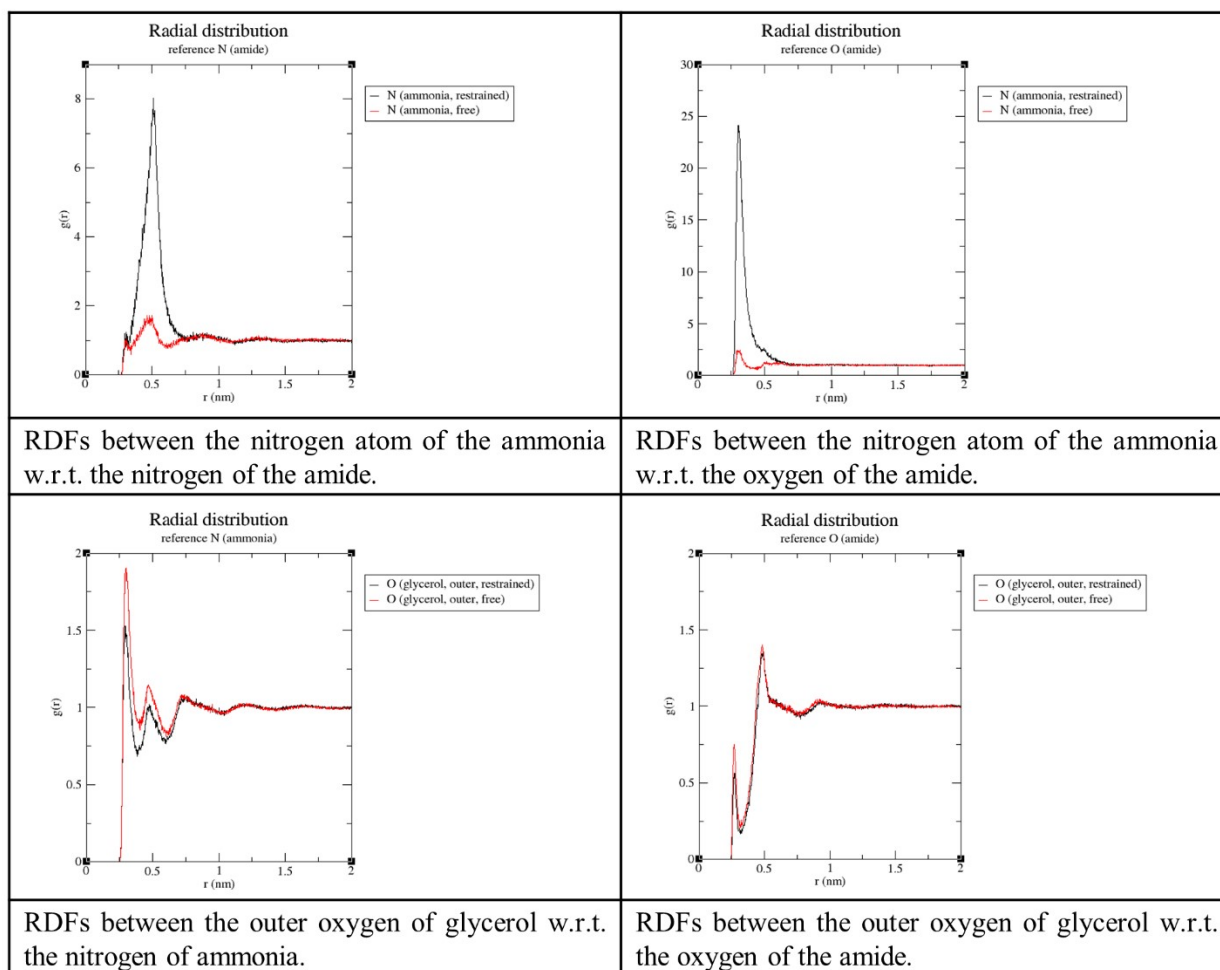tants' coordinates in place. In the second simulation, the ammonia and the amide were placed randomly in the solvent box and all atoms were allowed to move freely along the MD trajectory. The RDFs computed from the first simulation were compared to the RDFs calculated from the unrestricted simulation, and it was seen that both simulations resulted in qualitatively identical RDFs (*i.e.* peaks appeared at the same distances, see Figure S10), vouching that the proposed geometry –initially based solely on chemical intuition- shown in Figure S9 is indeed the preferred configuration in glycerol, at least in terms of distancing.
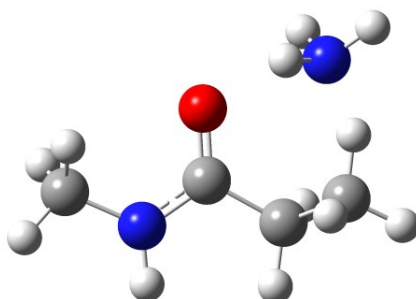

Figure S9. Geometry optimized amide-ammonia dimer at the b3lyp/6-31++g(d,p) level of theory including Grimme's D3 dispersion correction. Blue = nitrogen, red = oxygen, grey = carbon, white = hydrogen.
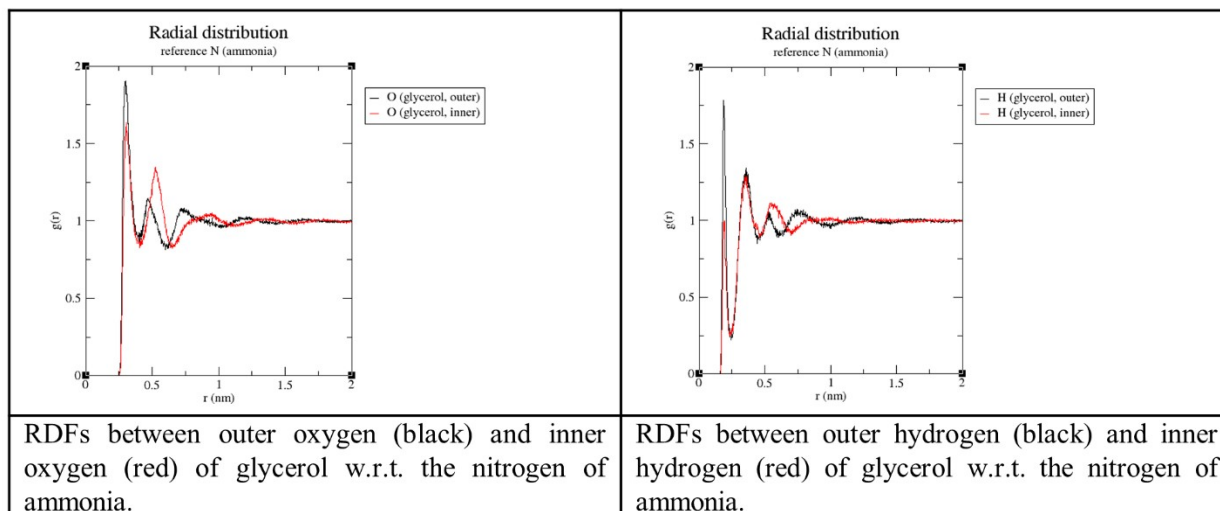
Radial distribution reference N (amide) (N (ammonia, restrained), N (ammonia, free))	Radial distribution reference O (amide) (N (ammonia, restrained), N (ammonia, free))
RDFs between the nitrogen atom of the ammonia w.r.t. the nitrogen of the amide.	RDFs between the nitrogen atom of the ammonia w.r.t. the oxygen of the amide.
Radial distribution reference N (ammonia) (O (glycerol, outer, restrained), O (glycerol, outer, free))	Radial distribution reference O (amide) (O (glycerol, outer, restrained), O (glycerol, outer, free))
RDFs between the outer oxygen of glycerol w.r.t. the nitrogen of ammonia.	RDFs between the outer oxygen of glycerol w.r.t. the oxygen of the amide.

Figure S10. Comparison between RDFs computed from the unrestricted simulation, versus the restricted simulation.

Continuing with the unrestricted simulation, RDFs involving glycerol w.r.t. the amide and ammonia compounds were examined in order to get an idea on how the glycerol molecules are oriented around the amide-ammonia pair. In the discussion set out below, the following nomenclature is adopted:
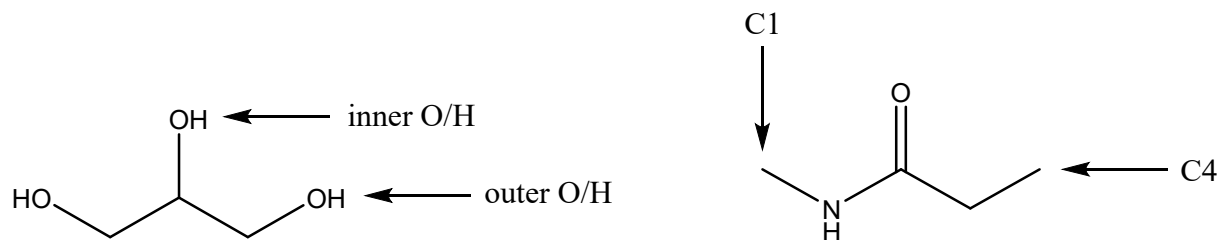

It should be noted that RDF$_{AB}$ = RDF$_{AC}$ if B and C are symmetrically equivalent. In that sense, the RDFs involving the two outer OHs in glycerol, and RDFs involving the three Hs of ammonia are indistinguishable.

22

| RDFs between outer oxygen (black) and inner oxygen (red) of glycerol w.r.t. the nitrogen of ammonia. | RDFs between outer hydrogen (black) and inner hydrogen (red) of glycerol w.r.t. the nitrogen of ammonia. |

Figure S11. RDFs between glycerol and ammonia.

From the figure above (Figure S11), it immediately becomes clear that there is a preferred proximity between glycerol and ammonia as indicated by well-defined peaks. The left plot shows that the preferred distance between ammonia's nitrogen and both the inner and outer oxygen atoms of glycerol is at 0.30 nm. Given that the highest peaks regarding the inner and outer oxygens appear at the same distance, it suggests that the ammonia is situated symmetrically w.r.t. said atoms. The RDF on the right shows a sharp peak at a distance of 0.19 nm representing the interatomic distance between the outer hydrogen of glycerol and ammonia's nitrogen. The preferred distance between the inner hydrogen of glycerol and ammonia's nitrogen is at a further distance of 0.36 nm. The combination of the peak at 0.19 nm seen on the right plot for the outer hydrogen, and the peak at 0.30 nm seen on the left plot for the outer oxygen suggests that a hydrogen bond is formed between the outer oxygen of glycerol as hydrogen bond donor and ammonia as hydrogen bond acceptor (as glycerol's outer H is in between O and N). This hypothesis is later confirmed by the NCI analysis. It should be noted that the left figure also shows a peak at a distance of 0.53 nm for the inner oxygen, albeit relatively small and broad. The coordination number at this distance equals 4 suggesting that this peak is not relevant for the configuration of the glycerol molecule in closest proximity of ammonia, as this peak results likely from a second solvation layer.
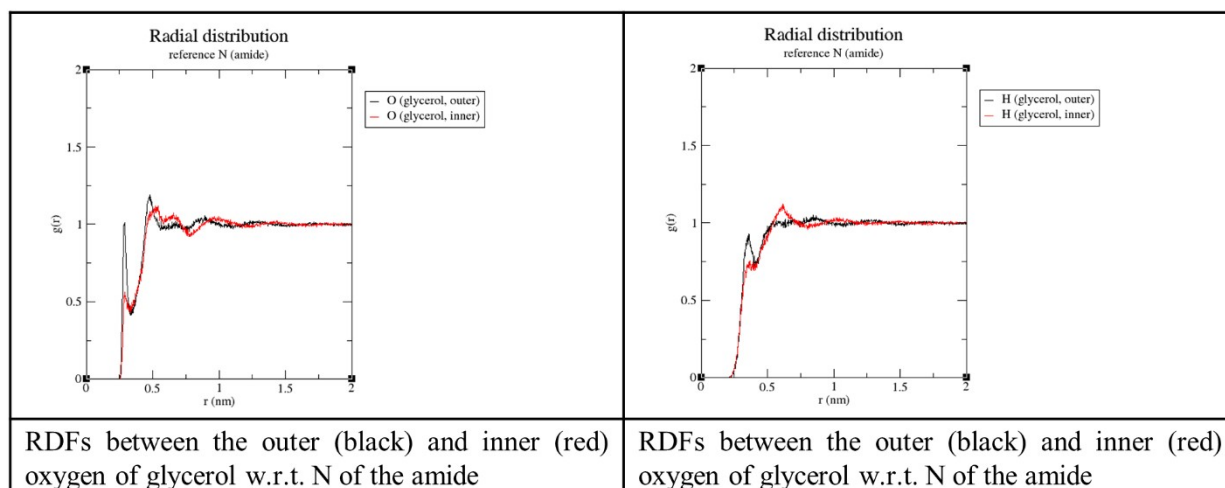
Figure S12. RDFs between glycerol and the amide.

The RDFs above (Figure S12) indicate that there is no interaction between glycerol's oxygens/hydrogens

and the amide's nitrogen (e.g. through hydrogen bonding) as there are no significant peaks where g(r) >

1. The RDFs below (Figure S13) indicate that glycerol is oriented along the NH-CH3 bond of the amide as

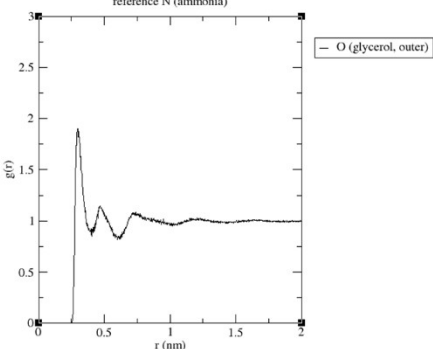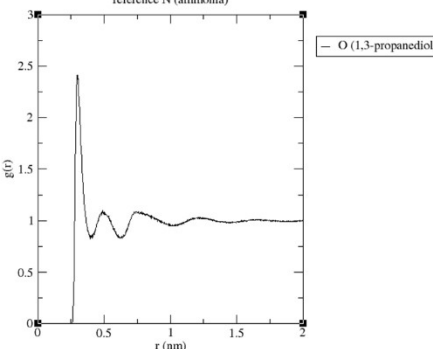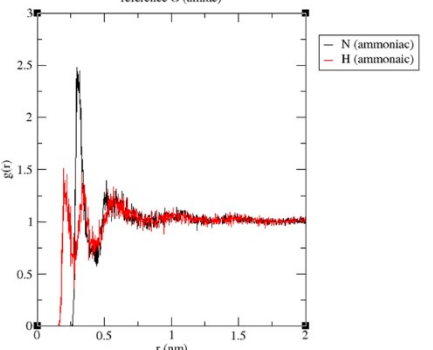the RDF on the right side indicates practically no preferred distancing.
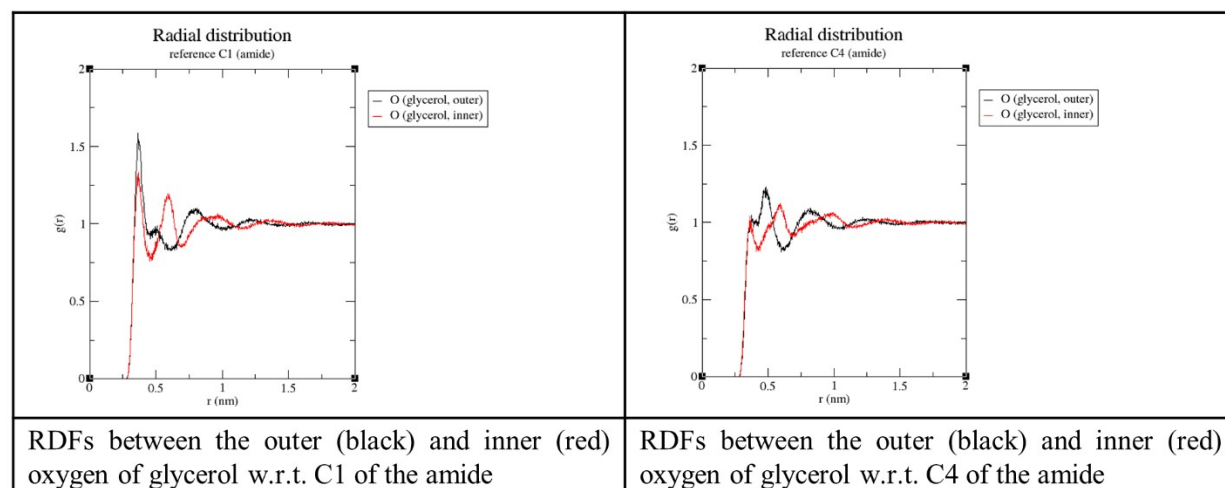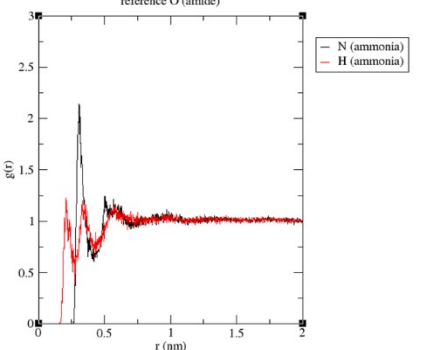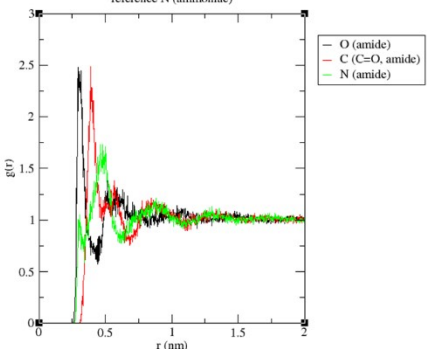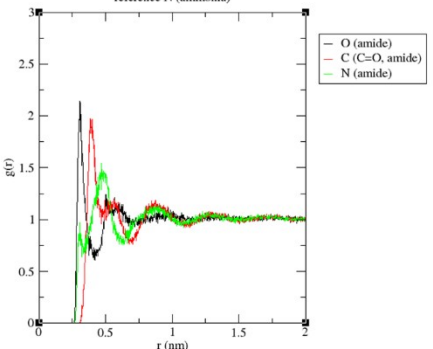

Figure S13. RDFs between glycerol and the amide (continued).
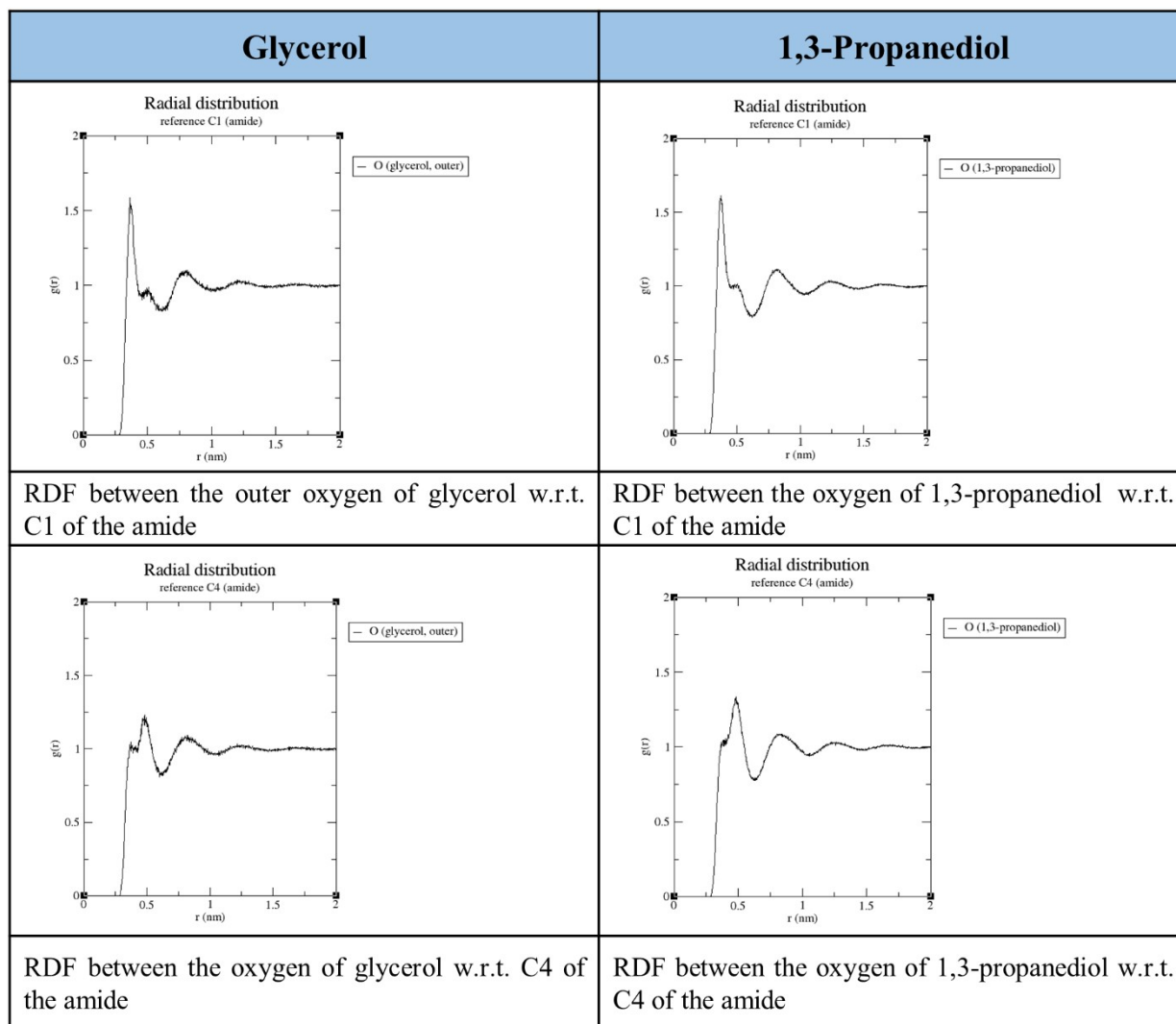
Reasoned by the discussion above, a well thought-out configuration (Figure S14) for the amide-ammonia-

glycerol complex was used as an initial guess for a geometry optimization using density functional theory

(DFT).
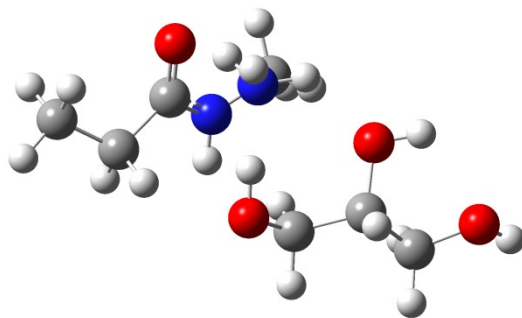
Figure S14. Geometry optimized amide-ammonia-glycerol complex at the b3lyp/6-31++g(d,p) level of theory including Grimme's D3 dispersion correction. Blue = nitrogen, red = oxygen, grey = carbon, white = hydrogen.

A simulation of the amide and ammonia in 1,3-propanediol was also started, and an RDF analysis was carried out similar to the examination explicated above (see Figure S15). Note that other than the peak heights, no significant difference is observed between the RDFs calculated in 1,3-propanediol compared to glycerol. It follows that 1,3-propanediol adopts a similar orientation to glycerol w.r.t. the amide-ammonia duo.

Glycerol	1,3-Propanediol
RDFs between outer oxygen glycerol w.r.t. the nitrogen of ammonia.	RDFs between oxygen of 1,3-propanediol w.r.t. the nitrogen of ammonia.
RDFs between nitrogen (black) and hydrogen (red) of ammonia and oxygen of the amide in glycerol	RDFs between nitrogen (black) and hydrogen (red) of ammonia and oxygen of the amide in 1,3-propanediol (bottom).
RDFs between the amide's oxygen (black), carbonyl carbon (red) and nitrogen (green) w.r.t. ammonia's nitrogen in glycerol.	RDFs between the amide's oxygen (black), carbonyl carbon (red) and nitrogen (green) w.r.t. ammonia's nitrogen in 1,3-propanediol.

Glycerol	1,3-Propanediol
RDF between the outer oxygen of glycerol w.r.t. C1 of the amide	RDF between the oxygen of 1,3-propanediol w.r.t. C1 of the amide
RDF between the oxygen of glycerol w.r.t. C4 of the amide	RDF between the oxygen of 1,3-propanediol w.r.t. C4 of the amide

Figure S15. Comparison between RDFs calculated in glycerol (left) and 1,3-propanediol (right).

The detection of the various non-covalent interactions in each optimized complex was achieved by means of a thorough Non-Covalent Interaction (NCI) analysis.[16] It allows identifying the non-covalent interactions by introducing a reduced density gradient s, defined as

$$s = \frac{|\Delta\rho|}{2k_f\rho}$$

where ρ is the electron density and k_f is the Fermi wave number, given by

$$k_f = \sqrt[3]{3\pi^2\rho}$$

Commonly, the reduced density gradient is plotted as a function of the electron density.

References

1.   K. Janssens, M. Stalpaert, M. Henrion and D. E. De Vos, *Chem. Commun.*, 2021, **57**, 6324-6327.

2.   R. A. Ford and H. S. B. Marshall, *J. Polym. Sci.*, 1956, **XXII** (101), 350-352.

3.   K. V. S. N. Raju and M. Yaseen, *J. Appl. Polym. Sci.*, 1991, **43** (8), 1533-1558.

4.   Huntingdon Fusion Techniques Limited, *Nylon chemical resistance and technical data*. Retrieved from: https://www.newmantools.com/pipestoppers/

5.   Carlisle, *Solvent & chemical resistance information*. Retrieved from: https://www.rfelektronik.se/manuals/Datasheets/solventguide

6.   S. R. Shukla, A. M. Harad and D. Mahato, *J. Appl. Polym. Sci.*, 2006, **100**, 186-190.

7.   Tosoh F-Tech Inc., *2,2,2-Trifluoroethanol (TFEA) Its Production Process and Various Applications*. Retrieved from: https://www.tosohusa.com

8.   R. Puffr and V. Kubanek, *Lactam-based Polyamides, Volume I Polymerization Structure*, CRC Press, 1991, pp. 100-106.

9.   B. Sun, *Chinese Journal of Polymer Science*, 1994, **12** (1), 57-65.

10.   R. Coeck, S. Berden and D. E. De Vos, *Green Chem.*, 2019, **21**, 5326-5335.

11.   J. H. Forsberg, V. T. Spaziano, T. M. Balasubramanian, G. K. Liu, S. A. Kinsley, C. A. Duckworth, J. J. Poteruca, P. S. Brown and J. L. Miller, *J. Org. Chem.*, 1987, **52**, 1017-1021.

12.   F. K. Behbahani, T. S. Daloee and P. Ziaei, *Current Organic Chemistry*, 2013, **7** (3), 296-303.

13.   R. J. McKinney, US5302756A, 1994.

14.   R. J. McKinney, US5395974A, 1995.

15.   R. Coeck, A. De Bruyne, T. Borremans, W. Stuyck and D. E. De Vos, *ACS Sustain. Chem. Eng.*, 2022, **10**, 9, 3048-3056.

16.   E. R. Johnson, S. Keinan, P. Mori-Sanchez, J. Contreras-Garcia, A. J. Cohen and W. Yang, *J. Am. Chem. Soc.*, 2010, **132**, 18, 6498-6506.